Early-onset behavioral and synaptic deficits in a mouse model of Alzheimer's disease

J. Steven Jacobsen*†, Chi-Cheng Wu‡, Jeffrey M. Redwine‡, Thomas A. Comery*, Robert Arias*, Mark Bowlby*, Robert Martone*, John H. Morrison‡§, Menelas N. Pangalos*, Peter H. Reinhart*, and Floyd E. Bloom†‡¶

*Discovery Neuroscience, Wyeth Research, CN-8000, Princeton, NJ 08543; ‡Neurome, Inc., La Jolla, CA 92037; and §Kastor Neurobiology of Aging Laboratories and Fishberg Department of Neuroscience, Mount Sinai School of Medicine, and ¶Department of Neuropharmacology, The Scripps Research Institute, La Jolla, CA 92037

Contributed by Floyd E. Bloom, February 7, 2006

Alzheimer's disease (AD) is a progressive neurodegenerative disorder for which numerous mouse models have been generated. In both AD patients and mouse models, there is increasing evidence that neuronal dysfunction occurs before the accumulation of β-amyloid (Aβ)-containing plaques and neurodegeneration. Characterization of the timing and nature of preplaque dysfunction is important for understanding the progression of this disease and to identify pathways and molecular targets for therapeutic intervention. Hence, we have examined the progression of dysfunction at the morphological, functional, and behavioral levels in the Tg2576 mouse model of AD. Our data show that decreased dendritic spine density, impaired long-term potentiation (LTP), and behavioral deficits occurred months before plaque deposition, which was first detectable at 18 months of age. We detected a decrease in spine density in the outer molecular layer of the dentate gyrus (DG) beginning as early as 4 months of age. Furthermore, by 5 months, there was a decline in LTP in the DG after perforant path stimulation and impairment in contextual fear conditioning. Moreover, an increase in the Aβ42/Aβ40 ratio was first observed at these early ages. However, total amyloid levels did not significantly increase until ≈18 months of age, at which time significant increases in reactive astrocytes and microglia could be observed. Overall, these data show that the perforant path input from the entorhinal cortex to the DG is compromised both structurally and functionally, and this pathology is manifested in memory defects long before significant plaque deposition.

β-amyloid | cognition

Alzheimer's disease (AD), a progressive neurodegenerative disease of the elderly, is the most common cause of dementia. Characteristic pathologies develop in the brain of AD patients, including senile plaques composed of β-amyloid (Aβ), neurofibrillary tangles composed of intracellular hyperphosphorylated microtubule-associated protein tau, as well as dystrophic neurites, diminished synaptic densities, and the loss of neuronal function (1). The amyloid hypothesis suggests that accumulation of Aβ fragments 1–40 and 1–42 is primarily responsible for AD pathology, and that it is the imbalance of Aβ production and Aβ clearance that appears to give rise to neurofibrillary tangle formation and the cognitive impairments associated with AD (2, 3).

To better understand disease progression, human amyloid precursor protein (APP) transgenic mouse lines expressing various mutations identified from patients with familial AD have been developed to model the effect of Aβ production and deposition on glial and neuronal structure and function and on cognitive performance (4–6). These models have become crucial to understanding the role of Aβ in AD pathology and for testing novel therapeutic strategies. To test the effects of candidate therapeutic treatments, it is necessary to recognize the type, extent, and onset of pathologies in each model. Variability across models largely reflects the background strain of the mouse and the characteristics of the molecular construct encoding mutant human APP (7). The influence of age and the spatial and temporal cumulative pathophysiological changes responsible for neurologic and behavioral deficits remain unknown.

Previous experiments using immunostaining, thioflavin fluorescence, and 3D reconstruction analyses to define the temporal and spatial events of Aβ accumulation and deposition in one transgenic mouse model of AD (PDAPP mice) demonstrated that, although amyloid deposits appear between 12 and 15 months of age throughout the cortex and hippocampal formation (8), a decreased volume of the dentate gyrus (DG) and a shortening of branches of dentate granule cells are apparent by 90 days of age (8, 9). These preamyloid deposition changes have been attributed to a selective vulnerability of dentate granule cells and the cells of the entorhinal cortex with projections that terminate in the molecular layer.

In contrast, in the Tg2576 transgenic (Tg) mouse model (originally termed $APP_{695}SWE$), amyloid plaques do not develop until 18 months (10), although both long-term potentiation (LTP) deficits in hippocampal CA1 and DG and spatial memory deficits in a modified water maze are detected at 6 months. This suggests impaired synaptic plasticity, because there was no observable loss of pre- or postsynaptic structural elements or neurons (11). Spatial memory deficits observed at 6 months were correlated with an elevation of detergent insoluble Aβ aggregates (12). Similarly, a preplaque reduction of synaptophysin had earlier been reported in another APP transgenic mouse strain at 2–3 months of age (13). This level of reduction can be correlated with APP expression and the age at which soluble Aβ levels rise in the mouse strain that expresses higher APP levels (14).

Here we have performed a systematic evaluation, from behavior to synaptic indices, of the temporal progression of neuronal dysfunction in the Tg mouse model of AD. We find that significant deficits in morphologic markers of synaptic integrity and behavior occur at 4 months, just before LTP deficits observed at 5 months and before the measurable rise of insoluble Aβ42 levels at 6 months. In contrast, as previously noted, amyloid plaque deposition in these animals is not detectable until 12–18 months of age. Measuring spine densities in the molecular layer of the DG using a modified stereologic approach to count spines in Golgi-impregnated neurons, we demonstrate a significant reduction of spine densities at 4 months of age that coincides with the first evidence of impaired hippocampal learning in contextual fear conditioning (CFC). Transgenic animals examined at younger ages do not display spine deficits nor were they impaired in the learning task. We conclude that a reduction in spine density correlating with CFC impairment

Conflict of interest statement: No conflicts declared.

Freely available online through the PNAS open access option.

Abbreviations: AD, Alzheimer's disease; Aβ, β-amyloid; APP, amyloid precursor protein; LTP, long-term potentiation; CFC, contextual fear conditioning; Tg, Tg2576 transgenic; I–O, input–output; DG, dentate gyrus.

†To whom correspondence may be addressed. E-mail: jacobss@wyeth.com or fbloom@scripps.edu.

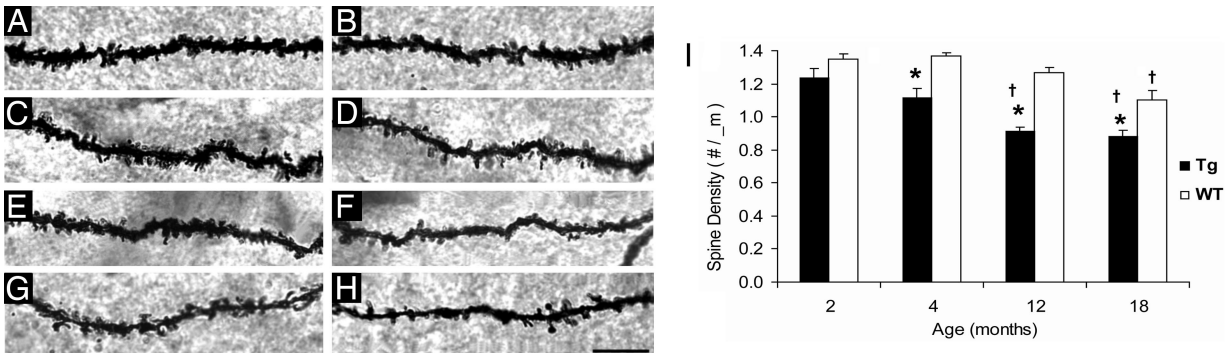

Fig. 1. Spine density in the DG. Spine segments are shown from 2-, 4-, 12-, and 18-month-old WT littermates (*A*, *C*, *E*, and *G*, respectively) and Tg mice (*B*, *D*, *F*, and *H*, respectively). Segments are from the molecular layer of the DG (middle and outer molecular layers combined). (Scale bar, 10 μm.) (*I*) Spine deficits were detected in 4-, 12-, and 18-month-old Tg mice compared with WT littermates but not in 2-month-old Tg mice (*, $P < 0.05$). Also shown is a reduced spine density detected over time in Tg mice and WT littermates (†, $P < 0.05$; see *Results* for specific comparisons).

is the earliest evidence of neuronal dysfunction observed in this mouse model of AD.

Results

Spine Density Is Decreased in Tg Mice. Using a modified stereological procedure, the spine density (i.e., number of spines per unit length of dendrite) of the outer-to-middle molecular layers of the DG was analyzed in 2-, 4-, 12-, and 18-month-old Tg and WT mice. The results showed both transgene- and age-dependent declines in spine density ($P < 0.0001$). No statistically significant difference in spine density was found between 2-month-old Tg and WT mice (although a marginal reduction of 8% was shown in 2-month-old Tg mice). A significant reduction (18%) in spine density was found in 4-month-old Tg compared with WT mice ($P < 0.0001$). In 12-month-old Tg mice, the reduction was also significant, and the deficit in Tg mice increased to 27% compared with that of WT mice ($P < 0.0001$). However, this deficit in spine density did not decline further between 12 and 18 months of age in Tg mice yet remained lower compared with WT mice (19% reduction, $P < 0.0001$). Within WT mice, a significant reduction in spine density was also found between 12 and 18 months, suggesting that the aging process itself can result in a loss of spines, with the degree of deficit increasing and occurring earlier in the APP transgenic mice (Fig. 1).

Basal Synaptic Transmission and LTP Reduced. ***Input–output (I–O) curve.*** In slices prepared from 2-month-old Tg mice, baseline synaptic transmission as measured by I–O curves is not significantly different from those of WT controls ($P > 0.05$). The maximum excitatory postsynaptic potential slope ± SEM was 4.2 ± 0.2 for WT [$n = 7(6)$] and 4.0 ± 0.3 for Tg [$n = 8(5)$] mice (Fig. 2*A*). In contrast, the I–O

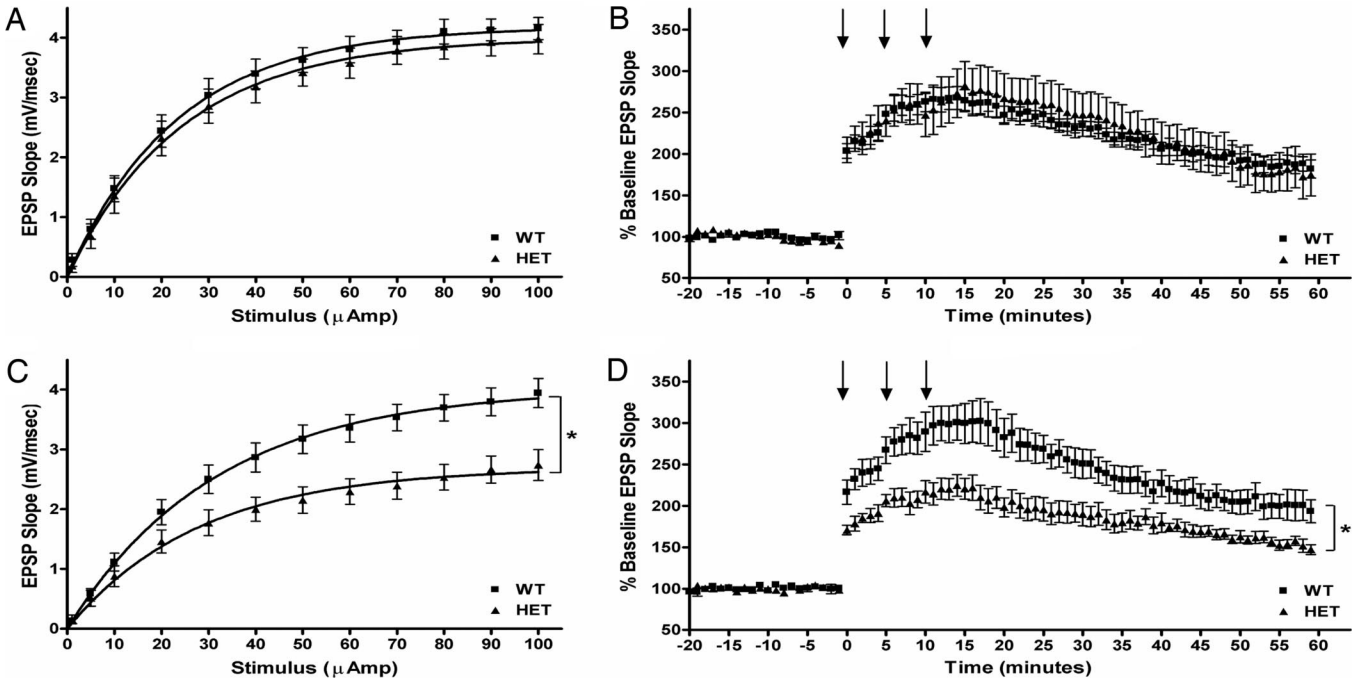

Fig. 2. Basal synaptic transmission and LTP. The DG is synaptically impaired in 4- but not 2-month-old Tg mouse hippocampal slices. (*A*) I–O curves were derived from dendritic recordings of the DG after step-wise increases in perforant path stimulation. No difference was found between 2-month-old Tg and WT slices. (*B*) LTP was induced by multiple high-frequency stimulus trains. The level of potentiation was comparable between 2-month-old Tg and WT slices. (*C*) The I–O curves of 4- to 5-month-old slices were significantly impaired compared with age-matched WT controls. (*D*) Slices from 4- to 5-month-old Tg mice potentiated significantly less than those from age-matched WT controls. In *B* and *D*, arrows indicate application time points of conditioning stimulus trains. In *C* and *D*, statistical significance is denoted (*, $P < 0.01$).

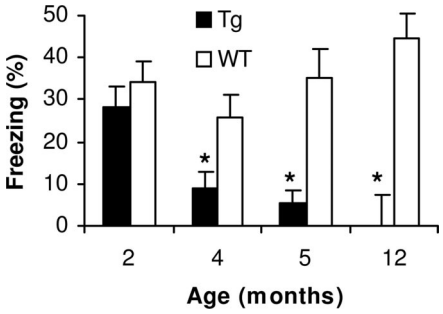

Fig. 3. Age-associated impairment in CFC. Tg mice display intact contextual memory at 2 months of age. A significant impairment in hippocampal-dependent conditioning is observed with lower levels of freezing to context at 5-month-old Tg mice when compared with younger ages (*, $P < 0.05$) with a trend toward an impairment in the 4-month-old group (†, $P = 0.05$). No differences were observed in freezing to context in the WT animals across all ages examined.

responses of 4- to 5-month-old Tg mouse slices showed a meaningful deficit when compared with those of their age-matched WT controls ($P < 0.01$). The maximum slope for these animals was 3.9 ± 0.25 for WT [$n = 8(4)$] and 2.7 ± 0.3 for Tg [$n = 13(7)$] mice (Fig. 2*C*).

LTP. LTP induction revealed age and genotype relationships comparable to those observed between the corresponding I–O curves. The response of 2-month-old Tg mouse slices to conditioning stimulus trains was not different from that of their WT controls ($P > 0.05$). For these animals, LTP ± SEM at 60 min was 186 ± 10% for WT [$n = 7(5)$] and 178 ± 27% for Tg [$n = 6(5)$] mice (Fig. 2*B*). In contrast, slices from 4- to 5-month-old Tg mice were significantly less responsive to conditioning trains than were slices from age-matched WT controls ($P < 0.001$). For these animals, LTP at 60 min was 199 ± 19% for WT [$n = 5(3)$] and 152 ± 6% for Tg [$n = 6(3)$] mice (Fig. 2*D*).

***In Vivo* Memory and CFC.** Contextual memory deficits were first observed in Tg mice beginning at 4–5 months of age. A significant difference is observed in 5-month-old mice, with less freezing exhibited with Tg than with WT mice ($P < 0.05$). In contrast, no significant difference in contextual memory is observed in 8- to 12-week-old Tg mice (Fig. 3).

Aβ Levels in Tg Brain. ***Aβ42 levels.*** Brain levels of Aβ peptide in the Tg mice were determined in 2- to 7-month-old animals by ELISA using Aβ40 and Aβ42 end-specific antibodies. The fraction of Aβ42 to total Aβ remained unchanged up to 6 months of age. However, between 6 and 7 months, the fraction of total Aβ made up by Aβ42 increases significantly to comprise >23% of the total Aβ level (Fig. 4).

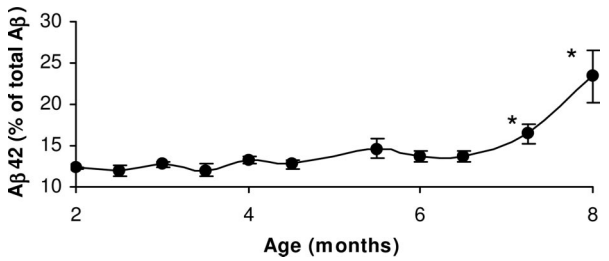

Fig. 4. Tg brain Aβ42 levels. Quantitative analysis of Aβ42 and Aβ40 levels extracted from Tg mouse brain. Brain Aβ42 and Aβ40 was measured by using sandwich ELISA in mice from 2- to 8-month-old animals. Statistical analysis indicates that the percentage of Aβ42 rises significantly after 7 months relative to total Aβ (Aβ40 and Aβ42) levels (*, $P < 0.05$).

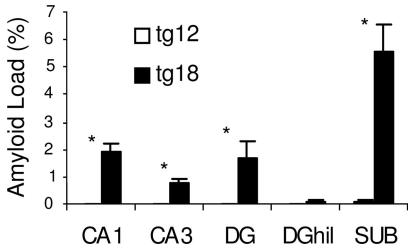

Fig. 5. Quantitative analysis of Aβ accumulation detected with 6E10. Caudal hippocampus is shown from 12- (on the left, open bars) and 18-month-old (on the right, closed bars) Tg mice. Significant Aβ accumulation was detected in 18-month-old mice in all subfields examined compared with minimal levels seen in 12-month-old mice. The subiculum contained significantly more Aβ compared with all other subfields ($P < 0.05$).

Amyloid load. Aβ accumulation in the Tg hippocampus was quantified by measuring amyloid load (volume fraction) of Aβ using monoclonal antibody 6E10 in 12- and 18-month-old transgenic Tg mice (15). Only occasional scattered plaques and therefore a very low or barely detectable amyloid load were observed in 12-month-old Tg mice. However, there was a significant increase in amyloid load in 18-month-old mice in the DG, CA1, CA3, and subiculum. The highest amyloid load was detected in the subiculum, followed by CA1, DG molecular layer, and CA3. There was almost no detectable amyloid load in the DG hilus of 18-month-old Tg mice (Fig. 5).

Astrocyte reactivity was measured by determining the volume fraction of GFAP immunoreactivity within each hippocampal subfield. Reactive astrocytes were observed only in restricted focal sites that matched the size and distribution of plaques as seen with 6E10 immunolabeling and thus were primarily observed in 18-month-old Tg mice. Reactive astrocytes were characterized by intense labeling with GFAP, large cell bodies, and shorter thicker processes compared with resting radial or stellate astrocyte morphology seen in WT tissue. The volume of each hippocampal subfield that contained more intensely labeled astrocytes above a set threshold was measured (see *Materials and Methods*). Eighteen-month-old Tg mice had a statistically significant increase in the GFAP volume fraction in the subiculum compared with age-matched WT mice ($P < 0.001$). Other subfields were not statistically different when comparing Tg mice with age-matched controls. Eighteen-month-old Tg mice had a statistically significant increase in GFAP volume fraction compared with 2-, 6-, or 12-month-old Tg mice, so there was an increase observed within the Tg group over time ($P < 0.001$). These differences were detected with multiple ANOVA main effects of age and genotype ($P < 0.001$) followed by post hoc tests (Fig. 7, which is published as supporting information on the PNAS web site).

Microglial reactivity was measured by determining the volume fraction of CD45 immunoreactivity within each hippocampal subfield. Activated microglia, characterized by short fat processes and an increase in CD45 staining intensity, were observed in restricted focal regions that matched the size and distribution of plaques as seen with 6E10 immunolabeling. This pattern resembled the pattern seen for reactive astrocytes. Eighteen-month-old Tg mice had a statistically significant increase in CD45 volume fraction compared with age-matched WT mice in the CA1, DG, and subiculum subfields ($P < 0.001$). There were no significant differences between Tg and WT mice at earlier ages. In addition, 18-month-old Tg mice had a statistically significant increase in CD45 volume fraction compared with Tg mice at all earlier ages (2, 6, and 12 months). These differences were detected with multiple ANOVA main effects of age and genotype ($P < 0.001$) followed by post hoc tests (Fig. 8, which is published as supporting information on the PNAS web site).

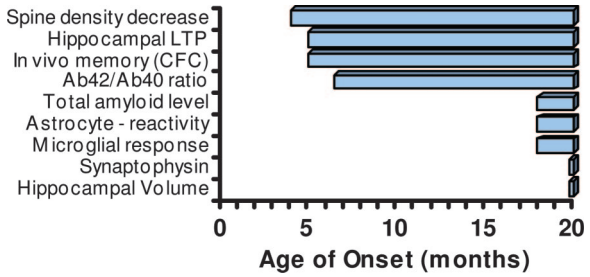

Fig. 6. Temporal progression of morphological and functional deficits in Tg mice. The earliest onset of deficits in these mice occurs at ≈4 months of age and includes a decrease in hippocampal spine density, LTP, and *in vivo* memory as measured by CFC, and an increase in the ratio of Aβ42/Aβ40. Slower onset deficits include an increase in amyloid load, reactive astrocytes, and microglia. No changes in synaptophysin staining or hippocampal volume were observed at any age up to 18-month-old animals.

Synaptophysin. Potential presynaptic changes within the hippocampus were measured by using stereologically based densitometric quantitation. No significant differences were detected between genotypes at any age. Six-month-old WT mice had a lower synaptophysin density in the CA1 and CA3 subfields compared with 12-month-old WT mice ($P < 0.05$) (Fig. 9, which is published as supporting information on the PNAS web site).

Hippocampal Volume. Volumes of DG, DG hilus, CA1, CA3, and subiculum were obtained from 2-, 6-, 12-, and 18-month-old Tg and WT mice. Twelve-month-old Tg mice had a significantly reduced DG volume compared with 12-month-old WT mice. However, 18-month-old Tg mice did not have a significantly reduced DG volume compared with WT mice. Other hippocampal regions measured also were not different between Tg and WT mice (Fig. 10, which is published as supporting information on the PNAS web site).

Discussion

This study demonstrates that neuronal deficits in Tg mice are established in a time-dependent manner and can be temporally clustered into early deficits observed in 4- to 5-month-old animals and late deficits observed in animals older than 12 months, as summarized (Fig. 6). The earliest observed changes include a decrease in spine density, deficits in hippocampal neurotransmission and LTP, *in vivo* memory deficits as measured by CFC, and an increase in the fraction of Aβ42 generated in brain.

The reduction in spine density seen in the outer molecular layer of the DG of heterozygous Tg mice is significant because, (*i*) it identifies an early reflection of pathology at an age and with a level of rigorous quantitation that has not been previously reported and that could be exploited as a potential indicator of therapeutic interventions, and (*ii*) it is a sensitive neuroanatomical substrate for the impairments in memory and LTP seen in this amyloid-based mouse model of AD, effectively modeling the early memory defects seen in humans with AD.

The decrease in spine density observed in the outer molecular layer of the Tg animals and the changes in synaptic physiology within the same region are consistent with the alterations in dendritic branching observed in the same brain region of another transgenic model of AD, the PDAPP mice (16). These data suggest that dysfunction of the circuitry of the outer molecular layer of the dentate is one of the earliest neuroanatomical effects of APP overexpression. In addition to data from murine AD models, molecular, neuroanatomical, and functional imaging studies of aging in rats and non-human primates suggest that this region is among the most sensitive to age-associated disruptions (17). Furthermore, AD patients display significant pathology within the outer molecular layer of the dentate and its afferent projection region in the entorhinal cortex beyond that observed with normal aging. For example, using quantitative electron microscopy, Scheff *et al*. (18) demonstrated a significant decrease in synapse density in the outer molecular layer of the DG occurs in AD patients relative to age-matched cognitively intact patients. In addition, as reviewed by Morrison and Hof (19), significant neuropathology is observed in the entorhinal cortex from AD patients, including significant neuronal loss and increased presence of extensive neurofibrillary tangles.

The functional changes during aging as well as the neuroanatomical changes associated with AD and AD mouse models suggest that the DG and its inputs from the entorhinal cortex may play a key role in age- and AD-associated cognitive deficits. Recent data examining the differing afferent projections of the entorhinal cortex suggest that the regional specificity of the observed alterations in neuroanatomy in young transgenic mice might underlie the observed memory deficits in the CFC paradigm. Hargreaves *et al*. (20) used single-unit recording of medial and lateral entorhinal cortical neurons in an attempt to characterize the spatial and nonspatial inputs into the hippocampus. Neurons of the medial entorhinal cortex displayed significant place field activity (i.e., a neuronal activity pattern correlated with the location of the animal in space), whereas very few neurons in the lateral entorhinal cortex displayed firing patterns correlated with spatial location. This separation of spatial and nonspatial inputs into the hippocampus is consistent with studies demonstrating specific deficits in spatial, but not contextual, learning after lesions of the afferents of the medial but not lateral entorhinal cortex (21). Lesions of the entorhinal cortex, and the lateral perforant path specifically, result in impaired CFC and altered contextual processing (22). The neuroanatomical and electrophysiological changes in the outer molecular layer of the DG in Tg potentially are the result of altered input from the lateral entorhinal cortex. These changes may give rise to the CFC deficits observed in the Tg mice. In older animals, however, reported deficits in spatial learning demonstrated using the Morris water maze are likely due to electrophysiological and neuroanatomical changes occurring within other regions of the hippocampal formation.

Deficits that occur after the early-onset changes discussed above include an increase in total amyloid load and in the number of reactive astrocytes and microglia. The long time interval among synaptic, electrophysiological, and behavioral deficits and plaque accumulation and gliosis was not expected and is important for understanding the course of disease and the development of therapeutic strategies beneficial to early treatment. Therapeutic interventions that protect against early deficits, such as reduced spine density, are important based on those deficits observed in human AD postmortem tissue (23–27). Additionally, the direct analysis of spine densities is likely to provide a more sensitive measure of synaptic numbers than densitometric analysis of synaptophysin immunoreactivity levels (28).

The induction of LTP deficits in rats *in vivo* (29) and in hippocampal slices by exposure to Aβ (30), the mitigation of such deficits either by immunodepletion of Aβ from slice medium (29) or by Aβ immunotherapy (31), and the pretreatment of Aβ solutions with proteolytic agents shown to selectively hydrolyze Aβ monomers (29) strongly implicate one or more forms of preplaque Aβ oligomer as being able to initiate neuronal dysfunction (5, 32, 33). Aβ peptides can disrupt LTP in hippocampus (11, 29, 34–37).

Interestingly, there appears to be a correlation between deficits in basal synaptic transmission or LTP observed in electrophysiological studies evaluating hippocampal synaptic plasticity in various young APP transgenic models and an increase in soluble Aβ levels (38, 39).

Overall, this study has highlighted the temporal progression of neuronal deficits observable in the Tg mouse model of AD. There is accumulating evidence that molecular, morphological, functional, and behavioral deficits can be measured for extended periods preceding the first evidence of plaque formation. In Tg animals, these changes occur at ≈4–5 months of age and include a significant

increase in the fraction of Aβ42 to Aβ40. Hence, the presence of one or more species of soluble Aβ containing an elevated proportion of Aβ42 may trigger some of the early-onset morphological and functional synaptic deficits that lead to memory dysfunction in this model. These data highlight the importance that early-intervention therapies will have in the treatment of AD.

Materials and Methods

Mice. Heterozygous male Tg mice (Swedish mutation Lys-670–Asn; Met-671—Leu) under the control of the prion promoter (10) and WT littermates were used for all studies. For volumetric and immunolabeling studies, six WT and six Tg mice were used at 2, 6, 12, and 18 months of age. For spine density analyses, five WT and five Tg mice were used at 2, 4, 6, and 12 months of age. CFC studies were performed on mice at 2, 3, 4, and 5 months of age ($n = 8$–18 per genotype per age).

Tissue Preparation. For volumetric and immunolabeling studies, mice were anesthetized with avertin (0.5 mg/g) and transcardially perfused with 10 ml of saline, followed by 100 ml of 4% paraformaldehyde in 0.1 M $NaPO_4$ buffer, pH 7.4, at 4°C. Brains were dissected, postfixed in 4% paraformaldehyde for 1 h, cryoprotected in 15% sucrose overnight followed by 30% sucrose overnight, then embedded and stored at −80°C. For spine density analysis, dissected brains were placed into Golgi impregnation solutions for 2 weeks.

Tissue Processing. For volumetric and immunohistochemical studies, coronal sections were obtained by using a freezing-stage sliding microtome. A series of evenly spaced 50-μm sections was taken for all analyses. For volumetric analysis, a one in eight series of sections was mounted onto gelatin-coated slides and stained with 0.1% thionin followed by 0.24% cresyl violet. Immunohistochemistry was performed on free-floating sections mounted on gelatin-coated slides. For spine density analysis, a one in two series of 100-μm-thick sections was analyzed after Golgi impregnation.

Antibodies. Biotinylated 6E10 (1:25,000; Signet Laboratories, Dedham, MA) was used for Aβ labeling, CD45 (1:25,000; Serotec) for microglia/macrophage/leukocyte labeling, GFAP (rabbit polyclonal, 1:25,000; DAKO) for astrocyte labeling, and synaptophysin (1:7,500; MAB5258, Chemicon) for labeling of presynaptic terminals and processes. Antibodies were diluted to ensure intermediate optical densities above background but below saturation.

Immunohistochemistry. Free-floating sections were incubated with primary antibody for 48 h, and biotinylated IgG secondary antibodies (0.25 μg/ml, Jackson ImmunoResearch) for 2 h. ABC kits were used for color substrate reactions (Vector Laboratories) followed by mounting and diaminobenzidine incubation for 7 min. Slides were dehydrated, cleared, and covered with DPX mountant (Fisher). Tissue sections from 2- and 6-month-old mice were assayed simultaneously and tissue sections from 12- and 18-month-old mice processed simultaneously.

Quantitative Immunohistochemistry and Volume Assessments. ***Acquisition of digital images.*** NeuroMosaic (Neurome, La Jolla, CA) was used to control an eight-slide motorized stage (Ludl, Hawthorne, NY) on a Zeiss Axioplan 2ie with a ×1.25 objective [numerical aperture (N.A.) = 0.035; final magnification, ×66; 5.2 μm per pixel] for Nissl stain or ×2.5 objective (N.A. = 0.12; final magnification, ×33; 2.6 μm per pixel). NeuroMosaic images were generated from image tiles acquired with an AxioCam HRc (Zeiss, Thornwood, NY). Analyses were performed blinded to genotype and age.
Volumes. Volume estimation was performed by using NEUROZOOMPRO (Nenrome) to apply contours of hippocampal subfields onto brain sections (400-μm interval). Contours were drawn to delineate CA1/CA2, CA3, DG, hilus of DG, and subiculum. Volumes of each subfield were estimated by using the Cavalieri principle, and a coefficient of error was calculated for each subfield to ensure a value of ≤0.1.
Densitometry. Densitometry (applied to synaptophysin) was performed by using NEUROZOOMPRO. Contours were drawn as described above. For each animal, a total relative optical density (ROD) was determined from all sections within each subfield. This was subtracted from background ROD taken from an intervening 1 in 24 series of sections that were unstained (primary antibody omitted) to give a specific ROD. A coefficient of error was calculated for each subfield, and a value of ≤0.1 was achieved for each subfield.

Volume fractions were used to estimate the percent of each hippocampal subfield that contained immunostaining (applied to Aβ, GFAP, and CD45) above a set gray-level threshold that was different for each label but constant for all mice. The threshold separated unstained and stained regions based on background levels in control unstained sections (primary antibody omitted). For 6E10, staining above threshold represented dense plaque regions. For GFAP and CD45, patterns of staining above threshold were intense within and around plaque-like regions and in cellular processes. Volumes for each subfield were estimated by using the Cavalieri principle and volume fractions calculated as the estimated volume of immunolabeling within each subfield divided by the total estimated volume for each subfield.

Golgi Impregnation Procedure and Spine Density Analysis. After cervical dislocation, brains were processed by using a Golgi-impregnation staining kit (FD Neurotechnologies, Ellicott City, MD). Brains were washed, coronally sectioned (100 μm) using a cryostat, mounted on adhesive microscope slides, and air-dried in the dark at room temperature. After 48 h, sections were rinsed, dehydrated, cleared of xylenes, and mounted onto ungelatinized glass slides. Slides were cover-slipped and allowed to dry before quantitative analysis. Extensive staining of many neurons throughout the DG was achieved. For dentate granule cells, spine density was measured on dendrites of the outer to middle molecular layers (O_MML). Using STEREOINVESTIGATOR (Microbrightfield, Williston, VT), unbiased stereological analyses were based on the principle of systematic random sampling. Spines were sampled within randomly chosen counting frames. The counting frame provided upper and lower guard zones and exclusion and inclusion boundaries. A one in two series of 100-μm sections was used to quantify the anterior–posterior axis of the DG. To secure the obtained data with minimal sampling error, the coefficient of error was constantly monitored to be <0.1. Golgi-impregnated neurons were numerous and evenly distributed enough to allow for systematic grid-based sampling of counting frames. In the DG, the O_MML was contoured under ×5 magnification based on the atlas as published (40). Spine counting required focusing in and out with the fine adjustment of the Axioplan microscope (Zeiss) using ×100 magnification and oil immersion. Only spines orthogonal to the dendritic shaft were readily resolved and included in this analysis, whereas spines protruding above or beneath the dendritic shaft were not sampled. Spine density was calculated by dividing the estimated number of total spines by the total length of dendritic segments within the counting frames and was expressed as the number of spines per micrometer of dendrite. For all 40 brains that were analyzed, the combined raw data include: 10,863 dendritic segments, 285,401 spines, and a total dendritic length of 7,135 μm. Densities of spines between Tg and WT mice of each age were compared by using univariate analysis of variance with Tukey HSD post hoc comparisons (SPSS, Chicago; $P < 0.05$).

Statistics. Anatomical data were analyzed by multiple ANOVA to test for statistically significant main effects or age × genotype interactions, followed by the Bonferroni post hoc test. Behavior results were analyzed by using a two-way ANOVA followed by post

hoc pairwise comparison made by using SAS statistical software (SAS Institute, Cary, NC).

Brain Aβ Measurement. Male Tg mice (8–32 weeks old) were saline-perfused and brains recovered and snap-frozen on dry ice. Brains were extracted as published (41). Brain Aβ40 and Aβ42 levels were measured by using a sandwich ELISA with 6E10 antibody (Signet Laboratories, Dedham, MA) for Aβ capture, and Aβ40 or Aβ42 C-terminal specific antibodies (Biosource International, Camarillo, CA) for detection. Aβ in experimental samples were compared with standard curves of synthetic Aβ peptides (Anaspec, San Jose, CA) to determine absolute Aβ levels.

Hippocampal Slice Electrophysiology. The procedure for hippocampal slice preparation and recording of extracellular field excitatory postsynaptic potential (FEPSP) I–O curves and LTP responses is described (42). Briefly, hippocampal slices were prepared from Tg heterozygous (HET) or WT mice, both 2 and 5 months of age. I–O curves were determined by 200-μsec stimuli increasing in intensity from 1 to 100 μA. Stimulus current was adjusted so that the field excitatory postsynaptic potential slope stabilized at 40–50% of maximum. Picrotoxin (30 μM) was perfused onto the slice for 30 min before LTP and throughout the experiment. After a 20-min baseline period, the first conditioning stimulus train consisted of high-frequency bursts (200 Hz) of 10 pulses each, repeated every 2 seconds for 10 cycles. Second and third conditioning trains were subsequently delivered, allowing 5 min of normal test pulse stimulation between trains. Stimulus pulses in the conditioning train were 400 μsec long or twice the test pulse duration. Raw I–O and baseline-normalized LTP fEPSP slope data were grouped according to age and genotype. For each age group, statistical significance between genotypes was tested by using a mixed-model repeated-measures analysis across all points on the I–O curves and across the postconditioning points on the LTP data sets. Sample sizes are given as the number of slices used in a data set, followed in parentheses by the number of animals from which they were prepared.

Behavioral Testing. Mice (n = 8–12 per genotype per age or treatment) were trained and tested in operant chambers on 2 consecutive days in the CFC paradigm, as described (43). Training consisted of two footshock (1.5-mA) presentations during a 5-min learning session, after which mice were removed from the chambers and returned to their home cages. Twenty hours after training, animals were returned to the training chambers. Freezing behavior was recorded by using time sampling in 10-sec bins for 5 min (30 sample points). Freezing was defined as lack of movement except that required for respiration. Approximately 1 h after this session, mice were placed into a novel environment, and freezing behavior was recorded for 3 min. Freezing scores for each animal were converted to percent freezing for each portion of the test. Memory for the context (contextual memory) for each animal was obtained by subtracting the percent freezing in a novel condition (a measure of basal activity) from that observed in the context.

1. Selkoe, D. J. (2000) *Ann. N.Y. Acad. Sci.* **924,** 17–25.
2. Hardy, J. & Selkoe, D. J. (2002) *Science* **297,** 353–356.
3. Bloom, G. S., Ren, K. & Glabe, C. G. (2005) *Biochim. Biophys. Acta* **1739**, 116–124.
4. Ashe, K. H. (2001) *Learn. Mem.* **8,** 301–308.
5. Morgan, D. (2003) *Neurochem. Res.* **28,** 1029–1034.
6. van Dooren, T., Dewachter, I., Borghgraef, P. & van Leuven, F. (2005) *Subcell. Biochem.* **38,** 45–63.
7. Bloom, F. E., Reilly, J. F., Redwine, J. M., Wu, C. C., Young, W. G. & Morrison, J. H. (2005) *Arch. Neurol.* **62,** 185–187.
8. Reilly, J. F., Games, D., Rydel, R. E., Freedman, S., Schenk, D., Young, W. G., Morrison, J. H. & Bloom, F. E. (2003) *Proc. Natl. Acad. Sci. USA* **100,** 4837–4842.
9. Redwine, J. M., Kosofsky, B., Jacobs, R. E., Games, D., Reilly, J. F., Morrison, J. H., Young, W. G. & Bloom, F. E. (2003) *Proc. Natl. Acad. Sci. USA* **100,** 1381–1386.
10. Hsiao, K., Chapman, P., Nilsen, S., Eckman, C., Harigaya, Y., Younkin, S., Yang, F. & Cole, G. (1996) *Science* **274,** 99–102.
11. Chapman, P. F., White, G. L., Jones, M. W., Cooper-Blacketer, D., Marshall, V. J., Irizarry, M., Younkin, L., Good, M. A., Bliss, T. V., Hyman, B. T., *et al.* (1999) *Nat. Neurosci.* **2,** 271–276.
12. Westerman, M. A., Cooper-Blacketer, D., Mariash, A., Kotilinek, L., Kawarabayashi, T., Younkin, L. H., Carlson, G. A., Younkin, S. G. & Ashe, K. H. (2002) *J. Neurosci.* **22,** 1858–1867.
13. Hsia, A. Y., Masliah, E., McConlogue, L., Yu, G. Q., Tatsuno, G., Hu, K., Kholodenko, D., Malenka, R. C., Nicoll, R. A. & Mucke, L. (1999) *Proc. Natl. Acad. Sci. USA* **96,** 3228–3233.
14. Mucke, L., Masliah, E., Yu, G. Q., Mallory, M., Rockenstein, E. M., Tatsuno, G., Hu, K., Kholodenko, D., Johnson-Wood, K. & McConlogue, L. (2000) *J. Neurosci.* **20,** 4050–4058.
15. Mayeux, R., Tang, M. X., Jacobs, D. M., Manly, J., Bell, K., Merchant, C., Small, S. A., Stern, Y., Wisniewski, H. M. & Mehta, P. D. (1999) *Ann. Neurol.* **46,** 412–416.
16. Wu, C. C., Chawla, F., Games, D., Rydel, R. E., Freedman, S., Schenk, D., Young, W. G., Morrison, J. H. & Bloom, F. E. (2004) *Proc. Natl. Acad. Sci. USA* **101,** 7141–7146.
17. Small, S. A., Chawla, M. K., Buonocore, M., Rapp, P. R. & Barnes, C. A. (2004) *Proc. Natl. Acad. Sci. USA* **101,** 7181–7186.
18. Scheff, S. W., Sparks, D. L. & Price, D. A. (1996) *Dementia* **7,** 226–232.
19. Morrison, J. H. & Hof, P. R. (1997) *Science* **278,** 412–419.
20. Hargreaves, E. L., Rao, G., Lee, I. & Knierim, J. J. (2005) *Science* **308,** 1792–1794.
21. Ferbinteanu, J., Holsinger, R. M. & McDonald, R. J. (1999) *Behav. Brain Res.* **101,** 65–84.
22. Burwell, R. D., Saddoris, M. P., Bucci, D. J. & Wiig, K. A. (2004) *J. Neurosci.* **24,** 3826–3836.
23. Moolman, D. L., Vitolo, O. V., Vonsattel, J. P. & Shelanski, M. L. (2004) *J. Neurocytol.* **33,** 377–387.
24. Spires, T. L. & Hyman, B. T. (2004) *Rev. Neurosci.* **15,** 267–278.
25. Jones, L. B. (2004) *Int. Rev. Neurobiol.* **59,** 1–18.
26. Fiala, J. C., Spacek, J. & Harris, K. M. (2002) *Brain Res. Brain Res. Rev.* **39,** 29–54.
27. Gertz, H. J., Cervos-Navarro, J. & Ewald, V. (1987) *Neurosci. Lett.* **76,** 228–232.
28. Calhoun, M., Jucker, M., Martin, L., Thinakaran, G., Price, D., Mouton, P. (1996) *J. Neurocytol.* **25,** 821–828.
29. Walsh, D. M., Klyubin, I., Fadeeva, J. V., Cullen, W. K., Anwyl, R., Wolfe, M. S., Rowan, M. J. & Selkoe, D. J. (2002) *Nature* **416,** 535–539.
30. Wang, H. W., Pasternak, J. F., Kuo, H., Ristic, H., Lambert, M. P., Chromy, B., Viola, K. L., Klein, W. L., Stine, W. B., Krafft, G. A., *et al.* (2002) *Brain Res.* **924,** 133–140.
31. Klyubin, I., Walsh, D. M., Lemere, C. A., Cullen, W. K., Shankar, G. M., Betts, V., Spooner, E. T., Jiang, L., Anwyl, R., Selkoe, D. J., *et al.* (2005) *Nat. Med.* **11,** 556–561.
32. Walsh, D. M. & Selkoe, D. J. (2004) *Neuron* **44,** 181–193.
33. Cleary, J. P., Walsh, D. M., Hofmeister, J. J., Shankar, G. M., Kuskowski, M. A., Selkoe, D. J. & Ashe, K. H. (2005) *Nat. Neurosci.* **8,** 79–84.
34. Zhao, D., Watson, J. B. & Xie, C. W. (2004) *J. Neurophysiol.* **92,** 2853–2858.
35. Gureviciene, I., Ikonen, S., Gurevicius, K., Sarkaki, A., van Groen, T., Pussinen, R., Ylinen, A. & Tanila, H. (2004) *Neurobiol. Dis.* **15,** 188–195.
36. Oddo, S., Caccamo, A., Shepherd, J. D., Murphy, M. P., Golde, T. E., Kayed, R., Metherate, R., Mattson, M. P., Akbari, Y. & LaFerla, F. M. (2003) *Neuron* **39,** 409–421.
37. Chen, Q. S., Wei, W. Z., Shimahara, T. & Xie, C. W. (2002) *Neurobiol. Learn. Mem.* **77,** 354–371.
38. Larson, J., Lynch, G., Games, D. & Seubert, P. (1999) *Brain Res.* **840,** 23–35.
39. Moechars, D., Dewachter, I., Lorent, K., Reverse, D., Baekelandt, V., Naidu, A., Tesseur, I., Spittaels, K., Haute, C. V., Checler, F., *et al.* (1999) *J. Biol. Chem.* **274,** 6483–6492.
40. Hof, P. R., Young, G. W., Bloom, F. E., Belichenko, P. V. & Celio, M. R. (2000) *Comparative Cytoarchitectonic Atlas of the C57BL/6 and 129/Sv Mouse Brains* (Elsevier, New York).
41. Johnson-Wood, K., Lee, M., Motter, R., Hu, K., Gordon, G., Barbour, R., Khan, K., Gordon, M., Tan, H., Games, D., *et al.*(1997) *Proc. Natl. Acad. Sci. USA* **94,** 1550–1555.
42. Day, M., Sung, A., Logue, S., Bowlby, M. & Arias, R. (2005) *Behav. Brain Res.* **164,** 128–131.
43. Comery, T. A., Martone, R. L., Aschmies, S., Atchison, K. P., Diamantidis, G., Gong, X., Zhou, H., Kreft, A. F., Pangalos, M. N., Sonnenberg-Reines, J., *et al.* (2005) *J. Neurosci.* **25,** 8898–8902.